Appl Phys B (2009) 94: 103–117
DOI 10.1007/s00340-008-3278-x

Applied Physics B
Lasers and Optics

Derivation of a temperature-dependent accommodation coefficient for use in modeling laser-induced incandescence of soot

H.A. Michelsen

Received: 26 June 2008 / Revised version: 9 October 2008 / Published online: 11 November 2008

Abstract This paper presents a derivation of an expression to estimate the accommodation coefficient for gas collisions with a graphite surface, which is meant for use in models of laser-induced incandescence (LII) of soot. Energy transfer between gas molecules and solid surfaces has been studied extensively, and a considerable amount is known about the physical mechanisms important in thermal accommodation. Values of accommodation coefficients currently used in LII models are temperature independent and are based on a small subset of information available in the literature. The expression derived in this study is based on published data from state-to-state gas-surface scattering experiments. The present study compiles data on the temperature dependence of translational, rotational, and vibrational energy transfer for diatomic molecules (predominantly NO) colliding with graphite surfaces. The data were used to infer partial accommodation coefficients for translational, rotational, and vibrational degrees of freedom, which were consolidated to derive an overall accommodation coefficient that accounts for accommodation of all degrees of freedom of the scattered gas distributions. This accommodation coefficient can be used to calculate conductive cooling rates following laser heating of soot particles.

PACS 65.80.+n · 78.20.Nv · 42.62.-b · 44.05.+e

H.A. Michelsen (✉)
Combustion Research Facility, Sandia National Labs, Livermore, CA, USA
e-mail: hamiche@sandia.gov
Fax: +1-925-2942276

1 Introduction

Laser-induced incandescence (LII) has become a popular technique for non-invasive measurements of soot concentration and primary particle size for a variety of applications. This technique involves heating particles with a high-power pulsed laser and collecting the radiative emission from the hot particles. The intensity of the signal depends on the particle volume fraction, making LII a useful tool for measuring soot spatial and temporal distributions under a wide range of conditions [1–3].

The signal decay rate is predominantly controlled by the conductive cooling rate at low fluences and atmospheric pressure. The conductive cooling rate, in turn, depends on the particle surface area to mass ratio. The correlation between this ratio and signal decay rate has been used extensively to infer primary particle size [2, 3]. Quantitative determination of particle size requires a detailed understanding of the physical mechanisms that control the LII signal decay rate and particle cooling rate. A thorough description of the conductive cooling rate, in particular, is required for deriving accurate particle sizes from signal decay rates.

Considerable effort has been devoted to developing models capable of predicting LII signals in response to pulsed-laser heating over a range of fluences [4]. Current models solve the energy- and mass-balance equations to predict the temporal response of the particle to a single laser shot. LII models typically account for particle heating by laser absorption and cooling by conduction to surrounding gases, sublimation of carbon clusters, and emission of thermal radiation. Nevertheless, there are severe limitations in the fundamental understanding of LII signal generation and significant uncertainties in model predictions and measurement interpretations.

Large uncertainties are associated with the calculated conductive cooling rate. The rate of heat loss by conductive cooling is generally calculated under free-molecular flow conditions according to the expression [4]

$$Q_{\mathrm{Cond}} = \frac{\pi D^2 Z_{\mathrm{surf}}}{N_a} \alpha_T \left(C_V + \frac{R}{2} \right) (T_S - T_g) \tag{1}$$

or an equivalent expression, where D is the primary particle diameter, Z_{surf} is the collision rate of the gas with the particle in units of $\mathrm{s}^{-1}\,\mathrm{cm}^{-2}$, N_a is the Avogadro constant, C_V is the heat capacity of the gas at constant volume, R is the universal gas constant, T_S is the surface temperature, T_g is the gas temperature, and α_T is the thermal accommodation coefficient. The most significant uncertainties in this expression originate from the thermal accommodation coefficient, which is a measure of the energy transferred between a gas molecule and a surface during a molecule-surface interaction. The value of this parameter ranges from 0 (when gas-surface collisions are completely elastic) to 1 (when molecules interact with the surface for a sufficiently long time to become fully energetically equilibrated with the surface before leaving it). For lack of better information, current LII models use temperature-independent values for α_T, despite expectations that this parameter should be dependent on surface temperature and gas temperature [5, 6]. Some LII models use values of 0.07 [7], 0.18 [8], 0.25 [9], 0.37 [10, 11], and 1.0 [12] inferred from measured LII decay rates by fitting model predictions of signal decay rates to measured values and allowing α_T to be one of the adjustable parameters. LII models, however, have significant uncertainties beyond the accommodation coefficient, and the conditions for the measurements are difficult to control, making this approach indirect and unreliable. Other models use a value (0.3) based on the measured accommodation coefficient of N_2 interacting with a graphite surface at gas temperatures near room temperature and surface temperatures in the range of 1,220–1,270 K [13]. In this experiment rotational temperature gradients were measured as the room-temperature gas interacted with the hot surface; rotational and translational temperatures were assumed to be equilibrated with each other. Although graphite is a good surrogate for soot, and N_2 is a good surrogate for air, extrapolating this result to more relevant temperatures (gas temperatures of ~1,700–1,900 K for flames and surface temperatures of ~2,500–4,000 K) is not possible without additional information. This paper attempts to address this problem using information from molecular beam scattering measurements of molecules (particularly diatomic molecules, predominantly NO) on graphite surfaces.

Energy can be transferred between the molecule and the surface via coupling between the translational, rotational, and vibrational degrees of freedom of the molecule and surface phonons. The surface can also facilitate coupling between the degrees of freedom of the molecule striking it. There is a large body of literature presenting experimental and theoretical studies of internal and kinetic energy transfer between surfaces and gas molecules. Many of these studies focus on the accommodation and coupling of the translational, rotational, and vibrational degrees of freedom of molecules as they interact with the surface. These studies can be extremely helpful in understanding thermal accommodation in general. The extensive state-to-state measurements of NO scattered from a graphite surface provided by Häger, Walther, and coworkers [14–21] in particular are useful for predicting the behavior of the accommodation coefficient under a wide range of conditions. Despite the large number of experimental and theoretical studies of energy transfer between gas molecules and surfaces, this data set is the only one available for scattering from graphite surfaces that is complete enough to derive an accommodation coefficient and extrapolate it to different surface- and gas-temperature regimes.

This paper presents a derivation of an expression that accounts for the temperature dependence of the thermal accommodation of individual degrees of freedom of molecules colliding with the surface of a soot particle. The derivation is based on state-to-state gas-surface scattering data available in the literature for diatomic molecules (particularly NO) impinging on a graphite surface. The final expression allows surface temperature and gas temperature to be taken into account in estimating the accommodation coefficient to be used in LII models.

2 Method

Molecular beam studies have demonstrated that at low surface temperatures molecules or atoms impinging on a surface will often scatter into two distinct populations. One of these populations is representative of direct inelastic scattering that is not fully accommodated with the surface, and the other is characteristic of trapping–desorption in which molecules are physisorbed to a surface for sufficiently long that internal and kinetic energy of the molecule is more fully equilibrated with the surface. Molecules from a beam undergoing direct inelastic scattering tend to have a narrow velocity distribution in a near-specular direction, whereas molecules undergoing trapping–desorption have a broader, angularly diffuse distribution [22, 23].

Partitioning of scattered molecules into separate diffuse and quasi-specular populations has been observed for *tert*-butyl chloride [24], fluoroform (CHF_3) [24], N_2 [25], and NO [14–16, 23] scattered from graphite. At higher surface temperatures for which trapping probabilities are low, only the direct inelastic component is observed, resulting in a decrease in thermal accommodation with increasing surface temperature. This behavior has been observed for *tert*-butyl

chloride [24], CHF_3 [24], Ar [16], and NO [14–16] scattered from graphite. The diffuse component decreases rapidly between 200 and 730 K for *tert*-butyl chloride [24] and CHF_3 [24] and disappears at surface temperatures above ~400 K for Ar [16] and NO [14–16, 26, 27]. For NO scattered from graphite, the sticking probability has been shown to decrease to zero at about the same surface temperature at which the diffuse component disappears [28].

For surface temperatures at which only direct inelastic scattering is observed, translational accommodation coefficients (α_{Trans}) can be derived from beam energies and energy distributions of the direct inelastically scattered molecules using the definition for the accommodation coefficient, i.e.,

$$\alpha_{\mathrm{Trans}} = \frac{E_i - E_f}{E_i - 2k_B T_S}, \tag{2}$$

where E_i is the kinetic (i.e., translational) energy of the incident beam, E_f is the average translational energy of the scattered molecules, k_B is the Boltzmann constant, and T_S is the surface temperature [5, 29, 30]. Likewise, accommodation coefficients for vibrational (α_{Vib}) or rotational (α_{Rot}) degrees of freedom can be inferred from internal state distributions of the incident and scattered molecules using a modification of (2), i.e.,

$$\alpha_{\mathrm{Vib,Rot}} = \frac{T_i^{\mathrm{Vib,Rot}} - T_f^{\mathrm{Vib,Rot}}}{T_i^{\mathrm{Vib,Rot}} - T_S}, \tag{3}$$

where T_i is the effective vibrational or rotational temperature of the incident beam, and T_f is the effective vibrational or rotational temperature of the scattered molecules [5, 29, 30].

If the dataset for partial accommodation coefficients is sufficient, we can estimate an overall accommodation coefficient using the expression [31]

$$\alpha_T(U)\left(C_V + \frac{R}{2}\right) = \alpha_{\mathrm{Trans}}\left(C_V^{\mathrm{Trans}} + \frac{R}{2}\right) + \alpha_{\mathrm{Rot}} C_V^{\mathrm{Rot}} + \alpha_{\mathrm{Vib}} C_V^{\mathrm{Vib}}, \tag{4}$$

where C_V^{Trans} is the translational heat capacity of the impinging gas at constant volume, C_V^{Rot} is the corresponding rotational heat capacity, and C_V^{Vib} is the corresponding vibrational heat capacity. For open systems in which pressure is constant and enthalpy H (rather than energy U) is the parameter of interest [32], (4) can be written with respect to heat capacities at constant pressure, i.e.,

$$\alpha_T(H)\left(C_P + \frac{R}{2}\right) = \alpha_{\mathrm{Trans}}\left(C_P^{\mathrm{Trans}} + \frac{R}{2}\right) + \alpha_{\mathrm{Rot}} C_P^{\mathrm{Rot}} + \alpha_{\mathrm{Vib}} C_P^{\mathrm{Vib}}. \tag{5}$$

The only difference between (4) and (5) is that the translational accommodation coefficient is weighted slightly more heavily in (5) because C_P^{Trans} is larger than C_V^{Trans} by R. These heat capacities can be approximated according to

$$C_V^{\mathrm{Trans}} = \frac{3}{2}R, \tag{6}$$

$$C_P^{\mathrm{Trans}} = C_V^{\mathrm{Trans}} + R = \frac{5}{2}R, \tag{7}$$

$$C_P^{\mathrm{Rot}} = C_V^{\mathrm{Rot}} = R, \tag{8}$$

$$C_P^{\mathrm{Vib}} = C_V^{\mathrm{Vib}} = R\left(\frac{\Theta_{\mathrm{Vib}}}{T}\right)^2 \frac{\exp(\frac{-\Theta_{\mathrm{Vib}}}{T})}{[1-\exp(\frac{-\Theta_{\mathrm{Vib}}}{T})]^2}, \tag{9}$$

where the effective "vibrational temperature" is given by [33]

$$\Theta_{\mathrm{Vib}} = \frac{\Delta E_{\mathrm{Vib}}}{k_B}, \tag{10}$$

where ΔE_{Vib} is the vibrational energy spacing (1,880 cm^{-1}) [15]. The overall thermal accommodation coefficient can thus be derived from α_{Trans}, α_{Rot}, and α_{Vib} using

$$\alpha_T(H) = \frac{3\alpha_{\mathrm{Trans}} + \alpha_{\mathrm{Rot}} + \alpha_{\mathrm{Vib}}\frac{C_P^{\mathrm{Vib}}}{R}}{4 + \frac{C_P^{\mathrm{Vib}}}{R}} \tag{11}$$

or

$$\alpha_T(U) = \frac{2\alpha_{\mathrm{Trans}} + \alpha_{\mathrm{Rot}} + \alpha_{\mathrm{Vib}}\frac{C_V^{\mathrm{Vib}}}{R}}{3 + \frac{C_V^{\mathrm{Vib}}}{R}}. \tag{12}$$

3 Results and discussion

3.1 Dependence of α_T on surface temperature

3.1.1 Dependence of α_{Rot} on surface temperature

Within experimental error the rotational accommodation coefficient for NO is unity at low surface temperatures of ≤300 K, i.e., temperatures at which molecules are predominantly diffusively scattered [14]. This observation is independent of initial rotational temperature and surface temperature. Figure 1a shows the rotational temperature of the scattered molecules as a function of surface temperature for beams with initial rotational temperatures of 20 and 35 K, first excited and ground-state vibrational states, incidence energies of 87.5 and 284 meV, and incidence angles of 30°, 60°, and 70°. The data are from Häger, Walther, and coworkers [15, 17, 18, 20, 21]. The data presented in Fig. 1a demonstrate that α_{Rot} is independent of vibrational state and incidence angle. Whereas at low surface

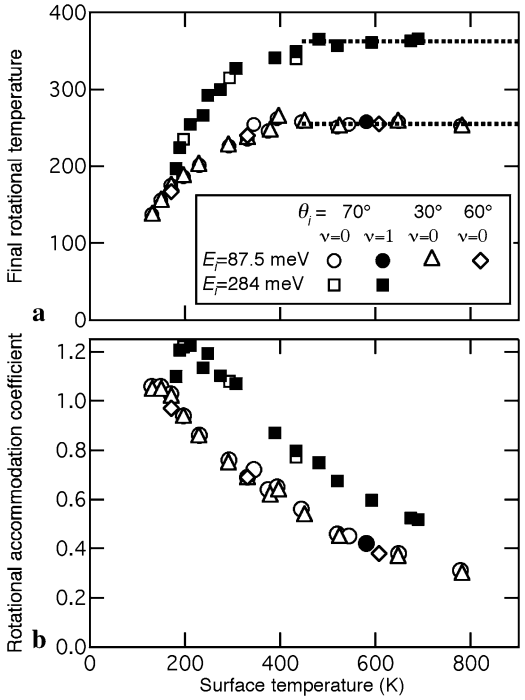

Fig. 1 Surface-temperature dependence of the rotational temperature and associated rotational accommodation coefficient of NO scattered from a graphite surface. (**a**) Final rotational temperatures and (**b**) rotational accommodation coefficients are shown as a function of surface temperature for several incidence angles, incidence energies, and initial vibrational states (see legend). *Squares* and *circles* represent values from Häger, Walther, and coworkers [20, 21], and *triangles* and *diamonds* signify values from Häger and Walther [17, 18]. The values are given in Table 1. The *dotted lines* in (**a**) represent the average value of measurements recorded at surface temperatures >400 K for each incidence energy

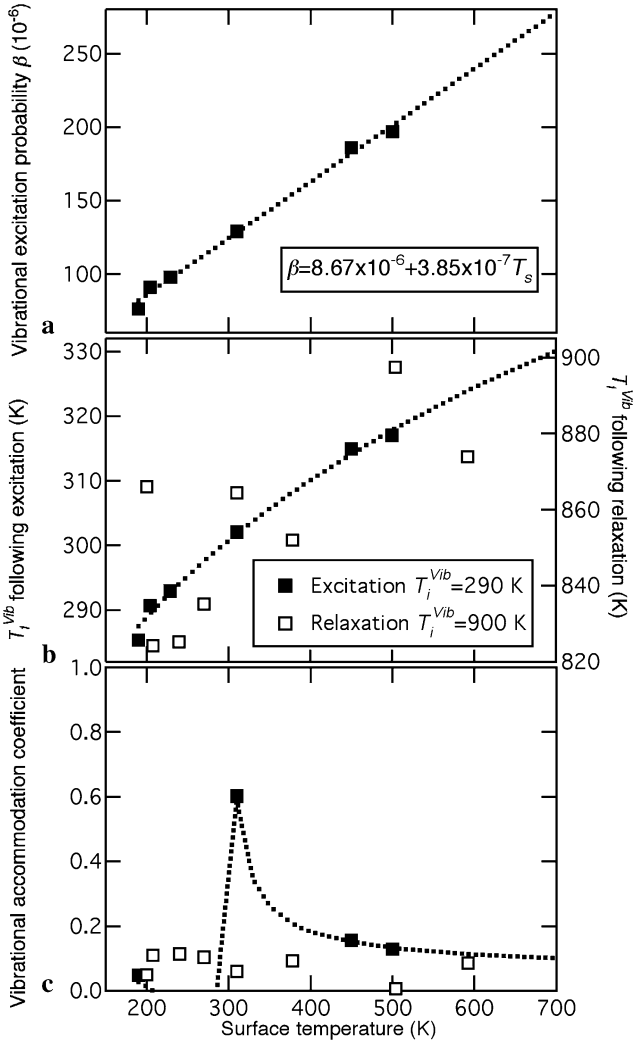

Fig. 2 Surface-temperature dependence of vibrational energy transfer for NO scattered from a graphite surface. (**a**) Vibrational excitation probabilities, (**b**) final vibrational temperatures, and (**c**) vibrational accommodation coefficients are shown as a function of surface temperature. The *solid squares* represent values for vibrational excitation of molecules with an initial vibrational temperature of 290 K from Vach et al. [15], and *open squares* represent values for vibrational relaxation of molecules with an initial vibrational temperature of 900 K from Vach et al. [20]. These values are given in Table 2. All data were recorded with an incidence energy of 284 meV and incidence angle of 70°. The *dotted lines* represent a linear fit to the vibrational excitation probability data in (**a**) and the corresponding (**b**) final vibrational temperature and (**c**) vibrational accommodation coefficient

temperatures the scattered molecules are rotationally fully accommodated with the surface ($T_f^{\mathrm{Rot}} \approx T_S$), at higher surface temperatures T_f^{Rot} is independent of T_S. This behavior has been reproduced using classical trajectory methods [34] and a statistical model approach [35]. Both simulation techniques suggest that it results from the conservation of the component of angular momentum normal to the surface. In the present study this behavior is used to extrapolate the results to higher surface temperatures, i.e., the final rotational temperature is assumed to be independent of T_S at surface temperatures higher than those measured, as indicated by the dotted lines in Fig. 1a. In the limit of high surface temperature this behavior yields an inverse surface temperature dependence for the rotational accommodation coefficient, i.e., $\alpha_{\mathrm{Rot}} \propto 1/T_S$ for large T_S. Figure 1b and Table 1 present values of α_{Rot} derived from the data shown in Fig. 1a. These data were from Fig. 2 of Vach et al. [20], Fig. 8 of Häger and Walther [21], and Fig. 5 of Häger and Walther [17, 18].

3.1.2 *Dependence of α_{Vib} on surface temperature*

Figure 2a shows the vibrational excitation probability of an NO molecule in its vibrational ground state scattered from a graphite surface. The data are from Fig. 8 of Vach et al. [15] for a beam of NO with an initial vibrational temperature of ~290 K, incidence energy of 284 meV, and incidence angle

Table 1 Rotational accommodation coefficients inferred from gas-surface scattering measurements on graphite over a range of surface temperatures

Species	T_S (K)	T_i^{Rot} (K)	T_f^{Rot} (K)	E_i (meV)	T_g (K)	α_{Rot}	Reference
NO	196	20	235	284	1,650	1.22	Fig. 2 of [20]
	293	20	315	284	1,650	1.08	Fig. 8 of [21]
	433	20	340	284	1,650	0.77	$(v=0) \rightarrow (v=0)$
NO	181	20	197	284	1,650	1.10	Fig. 2 of [20]
	189	20	224	284	1,650	1.21	Fig. 8 of [21]
	211	20	254	284	1,650	1.23	$(v=1) \rightarrow (v=1)$
	237	20	266	284	1,650	1.13	$\theta_i = 70°$
	248	20	292	284	1,650	1.19	
	274	20	300	284	1,650	1.10	
	307	20	327	284	1,650	1.07	
	389	20	341	284	1,650	0.87	
	433	20	349	284	1,650	0.80	
	481	20	365	284	1,650	0.75	
	519	20	357	284	1,650	0.68	
	592	20	361	284	1,650	0.60	
	674	20	363	284	1,650	0.52	
	689	20	366	284	1,650	0.52	
Extrapolated values	1,000	20	362	284	1,650	0.35	
	1,200	20	362	284	1,650	0.29	
	1,400	20	362	284	1,650	0.25	
	1,600	20	362	284	1,650	0.22	
	1,800	20	362	284	1,650	0.19	
	2,000	20	362	284	1,650	0.17	
	2,500	20	362	284	1,650	0.14	
	3,000	20	362	284	1,650	0.11	
	3,500	20	362	284	1,650	0.10	
	4,000	20	362	284	1,650	0.09	
	4,500	20	362	284	1,650	0.08	
	5,000	20	362	284	1,650	0.07	
NO	581	20	258	87.5	508	0.42	
NO	196	20	235	284	1,650	1.22	Fig. 2 of [20]
	293	20	315	284	1,650	1.08	Fig. 8 of [21]
	433	20	340	284	1,650	0.77	$(v=0) \rightarrow (v=0)$
NO	130	20	137	87.5	508	1.06	$\theta_i = 70°$
	148	20	156	87.5	508	1.06	
	170	20	175	87.5	508	1.03	
	196	20	186	87.5	508	0.94	
	230	20	201	87.5	508	0.86	
	292	20	226	87.5	508	0.76	
	330	20	235	87.5	508	0.69	
	344	20	254	87.5	508	0.72	
	374	20	254	87.5	508	0.64	
	393	20	246	87.5	508	0.65	
	444	20	262	87.5	508	0.56	
	519	20	258	87.5	508	0.46	
	544	20	251	87.5	508	0.45	
	648	20	258	87.5	508	0.38	
	778	20	253	87.5	508	0.31	

Table 1 (*Continued*)

Species	T_S (K)	T_i^{Rot} (K)	T_f^{Rot} (K)	E_i (meV)	T_g (K)	α_{Rot}	Reference
NO	131	35	135	87.5	508	1.04	Fig. 5 of [17, 18]
	149	35	153	87.5	508	1.04	$(v=0)\rightarrow(v=0)$
	171	35	173	87.5	508	1.01	$\theta_i = 30°$
	196	35	185	87.5	508	0.93	
	229	35	200	87.5	508	0.85	
	291	35	225	87.5	508	0.74	
	331	35	235	87.5	508	0.68	
	378	35	244	87.5	508	0.61	
	396	35	262	87.5	508	0.63	
	451	35	256	87.5	508	0.53	
	524	35	250	87.5	508	0.44	
	647	35	256	87.5	508	0.36	
	782	35	250	87.5	508	0.29	
NO	171	35	167	87.5	508	0.97	Fig. 5 of [17, 18]
	331	35	240	87.5	508	0.69	$(v=0)\rightarrow(v=0)$
	607	35	255	87.5	508	0.38	$\theta_i = 60°$

of 70°. The excitation probability is defined as

$$\beta = \frac{N(v=0 \rightarrow v=1)}{N(v=0)}, \tag{13}$$

where $N(v=0)$ represents the population of the vibrational ground state, and $N(v=0 \rightarrow v=1)$ represents the number of molecules excited from the ground state to the first excited vibrational state. This excitation probability is associated with a final vibrational temperature according to [15]

$$\beta = \exp\left(\frac{-\Delta E_{\mathrm{Vib}}}{k_B T_f^{\mathrm{Vib}}}\right). \tag{14}$$

The excitation probability is linearly dependent on surface temperature over the surface temperature measured. The data were extrapolated to higher surface temperatures by fitting the data in Fig. 2a and assuming a linear dependence at higher temperatures. Figure 2b shows the surface-temperature dependence of the final vibrational temperature estimated by rearranging (14), which gives

$$T_f^{\mathrm{Vib}} = \frac{-\Delta E_{\mathrm{Vib}}}{k_B \ln \beta}. \tag{15}$$

The dotted line is inferred from the linear fit to the data in Fig. 2a. Figure 2b also presents values of T_f^{Vib} derived from survival probabilities of vibrationally excited NO scattered from a graphite surface. Figure 3 of Vach et al. [20] provides survival probabilities of NO ($v=1$) in a beam with 5% vibrationally excited molecules also with an incidence energy of 284 meV and incidence angle of 70°. Multiplying these survival probabilities by 0.05 yields the population of vibrationally excited molecules scattered from the surface, the equivalent of β from which T_f^{Vib} is calculated. The values derived using these relaxation observations demonstrate considerably more scatter than those based on excitation experiments. The vibrational accommodation coefficients derived from these data are presented in Fig. 2c and Table 2. In contrast to the behavior shown for α_{Rot} in Fig. 1b, α_{Vib} decreases very gradually with increasing surface temperature. The large change near 300 K is related to the proximity of the surface temperature to the initial vibrational temperature of 290 K for the excitation experiments. Under such conditions, the accommodation coefficient is undefined.

Vibrational accommodation would be expected to be higher for larger molecular species, which have more vibrational modes and smaller vibrational spacings. This prediction is supported by values of α_{Vib} for CF_3Br scattered from graphite compared to extrapolated values for NO shown in Fig. 3. These values are also given in Table 2. They were derived from the results of Petterson and coworkers [36, 37] and demonstrate that the vibrational accommodation coefficient for CF_3Br/graphite decreases substantially with increasing surface temperature at surface temperatures of 500–1,200 K.

Andersson et al. [38] have noted that the vibrational temperature of SF_6 scattered from graphite demonstrates no dependence on surface temperature at high surface temperatures (950–1,400 K). This observation implies a decrease in the vibrational accommodation coefficient with increasing surface temperature, as shown in Fig. 3 and Table 2. Despite the large number of vibrational degrees of freedom, values of α_{Vib} derived from these data [38] are comparable to the extrapolated values for NO and significantly lower than those for CF_3Br at similar surface tem-

Table 2 Vibrational accommodation coefficients inferred from gas-surface scattering measurements on graphite over a range of surface temperatures

Species	T_S (K)	T_i^{Vib} (K)	T_f^{Vib} (K)	E_i (meV)	T_g (K)	α_{Vib}	Reference
NO	200	900	866	284	1,650	0.049	Fig. 3 of [20]
	208	900	824	284	1,650	0.110	
	240	900	825	284	1,650	0.113	
	270	900	835	284	1,650	0.103	
	310	900	864	284	1,650	0.060	
	378	900	852	284	1,650	0.092	
	504	900	898	284	1,650	0.006	
	592	900	874	284	1,650	0.085	
NO	190	290	285	284	1,650	0.047	Fig. 8 of [15]
	204	290	291	284	1,650	−0.008	
	229	290	293	284	1,650	−0.048	
	310	290	302	284	1,650	0.602	
	450	290	315	284	1,650	0.156	
	500	290	317	284	1,650	0.129	
Extrapolated values	600	290	324	284	1,650	0.111	
	800	290	336	284	1,650	0.090	
	1,000	290	345	284	1,650	0.078	
	1,200	290	353	284	1,650	0.069	
	1,400	290	360	284	1,650	0.063	
	1,600	290	367	284	1,650	0.058	
	1,800	290	373	284	1,650	0.055	
	2,000	290	378	284	1,650	0.051	
	2,500	290	390	284	1,650	0.045	
	3,000	290	400	284	1,650	0.041	
	3,500	290	410	284	1,650	0.037	
	4,000	290	418	284	1,650	0.035	
	4,500	290	426	284	1,650	0.032	
	5,000	290	433	284	1,650	0.030	
CF_3Br	830	320	427	690	4000	0.21	Table 1 of [36]
	1,170	320	466	690	4000	0.17	
CF_3Br	500	300	405	1600	9280	0.53	Fig. 6 of [37]
	600	300	400	1600	9280	0.33	
	800	300	440	1600	9280	0.28	
	1,000	300	475	1600	9280	0.25	
	1,200	300	500	1600	9280	0.22	
SF_6	950	300	318	640	3710	0.028	Fig. 2 of [38]
	1,170	300	318	640	3710	0.021	assuming T_f not
	1,400	300	318	640	3710	0.016	dependent on T_S
SF_6	950	300	346	1690	9810	0.071	
	1,170	300	346	1690	9810	0.053	
	1,400	300	346	1690	9810	0.042	

peratures and incidence energies. A study by van Opbergen et al. [39] has shown that at lower surface temperatures (178–425 K) the vibrational temperature of scattered SF_6 increases significantly with surface temperature [39], but their paper does not provide sufficient information to determine whether the vibrational accommodation

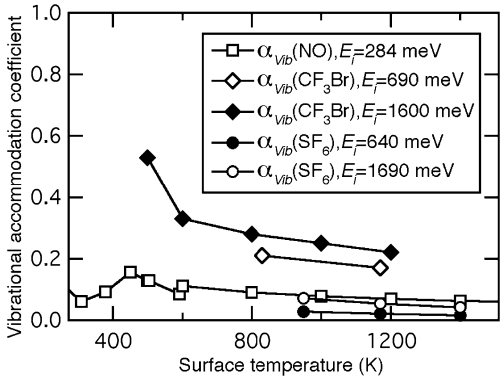

Fig. 3 Surface-temperature dependence of the vibrational accommodation coefficient for NO, CF_3Br, and SF_6 scattered from a graphite surface. The *squares* represent values derived and extrapolated from measurements of Vach et al. [15] recorded with an incidence angle of 70°. Values for CF_3Br were derived from data from Andersson et al. [36] (*open diamonds*) and Någård et al. [37] (*solid diamonds*) recorded with an incidence angle of 45°. Values for SF_6 were derived from data from Andersson et al. [38] (*circles*) recorded with an incidence angle of 21°. Incidence energies are given in the legend. Values of accommodation coefficients are given in Table 2

coefficient increases or decreases with surface temperature.

3.1.3 *Dependence of* α_{Trans} *on surface temperature*

Inferring translational accommodation coefficients from the available surface scattering data is more complicated than determining either rotational or vibrational accommodation coefficients. The extent of translational accommodation depends on incidence angle, which must be taken into account when determining the integrated accommodation coefficient. Translational accommodation also depends on scattering angle, which must be accounted for in the analysis when data are not collected at the peak of the angular distribution.

Figure 4a presents data from Fig. 6 of Vach et al. [21], which shows the peak of the time-of-flight velocity distribution as a function of surface temperature (open triangles). The data were measured with an incidence angle of 50°, a fixed scattering angle of 45°, and an incidence velocity of 1,350 m/s, which corresponds to an incidence energy of 284 meV. Figure 5 presents data from a number of studies [14, 16–19, 21] showing that the peak of the angular distribution of the scattered molecules decreases with increasing surface temperature. The data shown in Fig. 4a were recorded at an angle smaller than the peak of the scattered angular distribution. In addition, the velocity of the scattered molecules decreases with increasing scattering angle [15, 16, 20]. Hence, the measured velocities shown in Fig. 4a are higher than the most probable velocities for the scattered distributions.

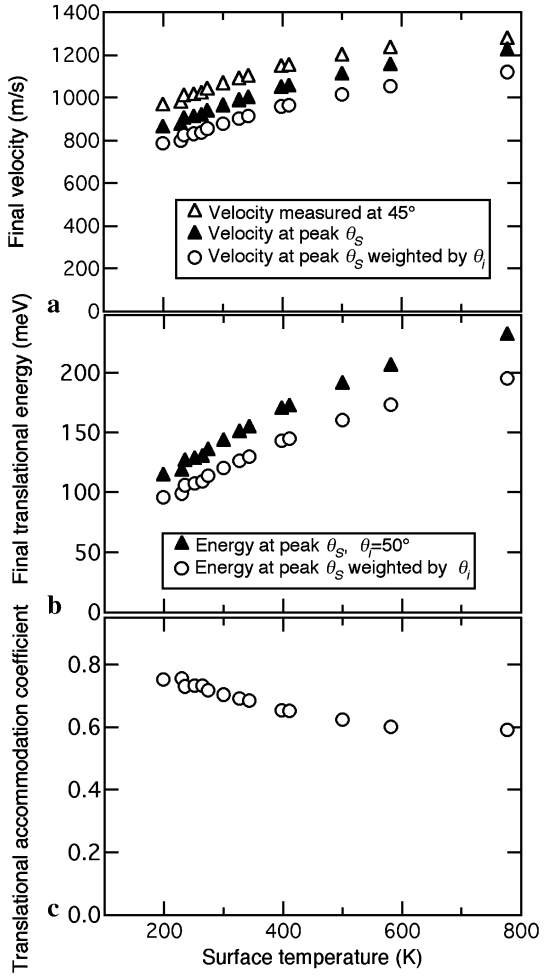

Fig. 4 Surface-temperature dependence of the (**a**) final velocity, (**b**) final translational energy, and (**c**) translational accommodation coefficient for NO scattered from a graphite surface (given in Table 3). The *open triangles* in (**a**) represent measurements of Vach et al. [15] recorded with an incidence angle of 50° and scattering angle of 45° with an incidence energy of 284 meV. The solid triangles in (**a**) and (**b**) show these measurements corrected to represent values at the peak scattering angle. The *circles* in each panel show the results corresponding to the initial measurements corrected for peak scattering angle and averaged over all incidence angles

The most probable velocity at a particular surface temperature can be estimated by first identifying the peak scattering angle at this surface temperature and then determining the velocity at this angle. Figure 5 shows that linear fits to several data sets of peak scattering angle vs T_S yield the same slope of −0.0175 deg/K. The peak scattering angle at each surface temperature can be derived for the data in Fig. 4a using this slope scaled to a value of 56°, the peak angle at 500 K derived from the data in Fig. 5 of Vach et al. [15]. The result is represented by the dotted curve in Fig. 5. Figure 6 shows the ratio of the velocity at the peak of the angular distribution relative to the velocity at some scattering angle as a function of the difference between that scattering angle and the peak angle. The

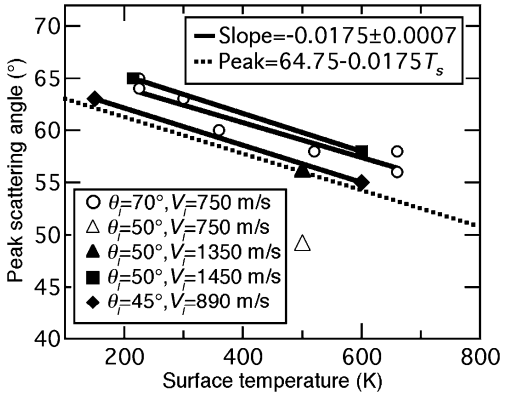

Fig. 5 Surface-temperature dependence of the peak scattering angle for NO scattered from a graphite surface. The symbols represent values from Häger et al. [16, 18] (*circles*), Häger and Walther [17] (*open triangle*), Vach et al. [15] (*solid triangle*), Kuze et al. [19] (*squares*), and Häger et al. [14] (*diamonds*). The *solid lines* represent linear fits to the data sets with more than one point. The *dotted line* represents a line with the slope given by the average of the three fits (*solid lines*), adjusted to pass through the *solid triangle*

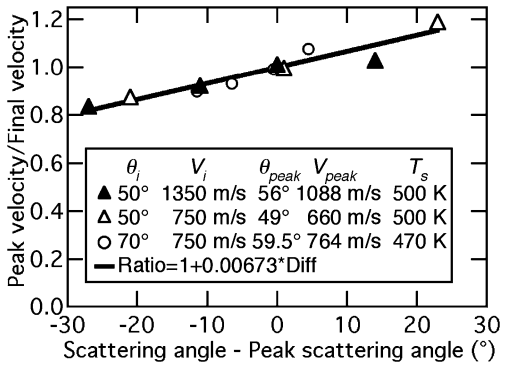

Fig. 6 Velocity at the peak of the angular distribution relative to the measured velocity as a function of the angular difference between the scattering angle at which the measurements were made and the peak of the angular distribution. The symbols represent values from Häger et al. [16] (*circles*), Häger and Walther [17] and Vach et al. [15] (*open triangles*), and Vach et al. [15] (*solid triangles*). The *solid line* represents a linear fit to the data sets combined

results are scaled to unity when the scattering angle is at the peak of the angular distribution. The results from several experiments fall along the same line with a slope of 0.00673/deg. The values of the peak scattering angle derived as a function of surface temperature in Fig. 5 were subtracted from the scattering angle (45°). This difference was then used to determine the ratio of the peak velocity relative to velocities at other angles. The measured velocities shown in Fig. 4a were multiplied by this ratio to convert the measured velocities to velocities at the peak scattering angle, and the results are compared to the original values in Fig. 4a. The velocities at the peak of the angular distribution were converted to energies and are displayed in Fig. 4b.

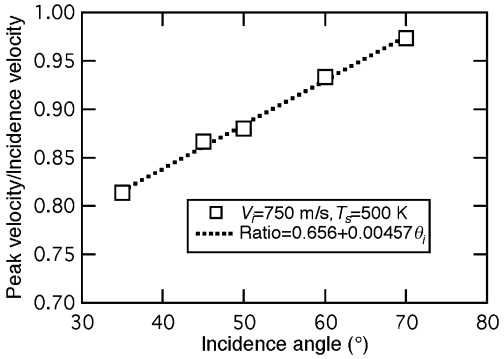

Fig. 7 Velocity at the peak of the angular distribution relative to the incidence velocity as a function of the incidence angle. The *symbols* represent values from Häger and Walther [17]. The *dotted line* represents a linear fit to the data

Because momentum parallel to the surface is more likely to be conserved during the gas–surface collision than momentum perpendicular to the surface, the incidence angle must also be taken into account in determining accommodation. Figure 7 shows a linear increase of the most probable velocity with increasing incidence angle. These results are scaled by the incidence energy and were derived from measurements of Häger and Walther [17]. Performing a linear fit to the data in Fig. 7 gives an intercept of 0.656 and a slope of 0.00457/degree or 0.262/radian. An average over incidence angle can be derived according to

$$\left\langle \frac{V_{\text{peak}}}{V_i} \right\rangle = \frac{\int_0^{\pi/2} (0.656 + 0.262\theta_i) \cos\theta_i \, d\theta_i}{\int_0^{\pi/2} \cos\theta_i \, d\theta_i} = 0.8055. \tag{16}$$

Dividing this average value by 0.88, the value for 50° (the incidence angle for the data in Fig. 4), gives a multiplicative correction factor of 0.92 for the dependence of the final velocity on incidence angle over all solid angles. The results are shown in Fig. 4a and presented as final kinetic energies in Fig. 4b. Figure 4c and Table 3 present the corresponding translational accommodation coefficients.

Previous work has suggested that the average final kinetic energy is linearly dependent on both incidence energy and surface temperature [40, 41], i.e.,

$$E_f = a_1 E_i + a_2 E_S, \tag{17}$$

where $E_S = 2k_B T_S$, and a_1 and a_2 are constants. Values of E_f shown in Fig. 4b, however, are not fit very well by this functional form. In this case E_i is constant (284 meV), and E_f appears to demonstrate saturation behavior at high surface temperatures. Figure 8a presents the results of fits using functions that follow the form of (17) in the limit of low surface temperature and start to saturate at high surface tem-

Table 3 Translational accommodation coefficients inferred from gas-surface scattering measurements on graphite over a range of surface temperatures

Species	T_S (K)	E_S (meV)	E_f (meV)	E_i (meV)	T_g (K)	α_{Trans}	Reference
NO	199	34	96	284	1,650	0.75	Fig. 6 of [15]
	230	40	99	284	1,650	0.76	
	235	41	106	284	1,650	0.73	
	251	43	108	284	1,650	0.73	
	264	45	109	284	1,650	0.73	
	274	47	114	284	1,650	0.72	
	300	52	120	284	1,650	0.70	
	327	56	127	284	1,650	0.69	
	343	59	130	284	1,650	0.69	
	398	69	143	284	1,650	0.65	
	411	71	145	284	1,650	0.65	
	500	86	161	284	1,650	0.62	
	581	100	174	284	1,650	0.60	
	777	134	195	284	1,650	0.59	
Extrapolated values	1,000	172	228	284	1,650	0.50	
	1,200	207	248	284	1,650	0.47	
	1,400	241	265	284	1,650	0.43	
	1,600	276	280	284	1,650	0.39	
	1,800	310	292	284	1,650	0.36	
	2,000	345	304	284	1,650	0.32	
	2,500	431	327	284	1,650	0.29	
	3,000	517	344	284	1,650	0.26	
	3,500	603	358	284	1,650	0.23	
	4,000	689	369	284	1,650	0.21	
	4,500	776	379	284	1,650	0.19	
	5,000	862	387	284	1,650	0.18	
N_2	1,245	215			293	0.26	[13]

perature. These functions are:

$$\text{Error function} \quad E_f = a_1 E_i + a_2 a_3 erf\left(\frac{E_S}{a_3}\right); \tag{18}$$

Exponential function

$$E_f = a_1 E_i + a_2 a_3 \left[1 - \exp\left(\frac{-E_S}{a_3}\right)\right]; \tag{19}$$

$$\text{Ratio} \quad E_f = a_1 E_i + a_2 \left(\frac{E_S}{1 + \frac{E_S}{a_3}}\right), \tag{20}$$

where a_3 is a constant. For these equations,

$$\lim_{E_S \to 0} E_f = a_1 E_i + a_2 E_S, \tag{21}$$

$$\lim_{E_S \to \infty} E_f = a_1 E_i + a_2 a_3. \tag{22}$$

The functions were fit to the θ_i-weighted data from Fig. 4b in addition to a point constrained to $E_f = 284$ meV at $E_S = E_i = 284$ meV. The best fit is provided by (20), as shown by the values of χ^2 for the results given in Table 4. Figure 8b presents the translational accommodation coefficients inferred from these fits compared with the values inferred from the measurements. The linear fit using (17) gives very poor agreement with the values inferred from the measurements, as expected from the poor fit provided by this function. The other fits give much better agreement with the inferred values and extrapolate to much lower values of α_{Trans} than estimated using the linear function. The deviations from a smooth curve near $T_S = 1{,}650$ K occur at the point where $E_f \approx E_S \approx E_i$. In the results presented below and in Table 3, α_{Trans} is extrapolated to higher surface temperatures using the best-fit function, i.e., (20), and values of α_{Trans} near $T_S = 1{,}650$ K have been interpolated.

The results in Fig. 8 demonstrate a decrease in α_{Trans} with increasing surface temperature for both the points inferred from the data and the extrapolated values. Other data sets that provide information for *t*-butyl chloride [24], CHF_3 [24], and Xe [42] scattered from graphite as a func-

Table 4 Results of fits of final kinetic energy E_f as a function of $E_S = 2k_B T_S$ for extrapolating α_{Trans} to higher surface temperatures

[a] $\chi^2 = \sum_j (E_{f,j}^{\text{measured}} - E_{f,j}^{\text{predicted}})^2$ for each point j

	a_1	a_2	a_3	χ^{2a}
$E_f = a_1 E_i + a_2 E_S$	0.289	0.758		1374
$E_f = a_1 E_i + a_2 a_3 \text{erf}(\frac{E_S}{a_3})$	0.198	1.095	223.0	174
$E_f = a_1 E_i + a_2 a_3 [1 - \exp(\frac{-E_S}{a_3})]$	0.157	1.667	180.2	103
$E_f = a_1 E_i + a_2 (\frac{E_S}{1+\frac{E_S}{a_3}})$	0.134	1.936	227.7	81

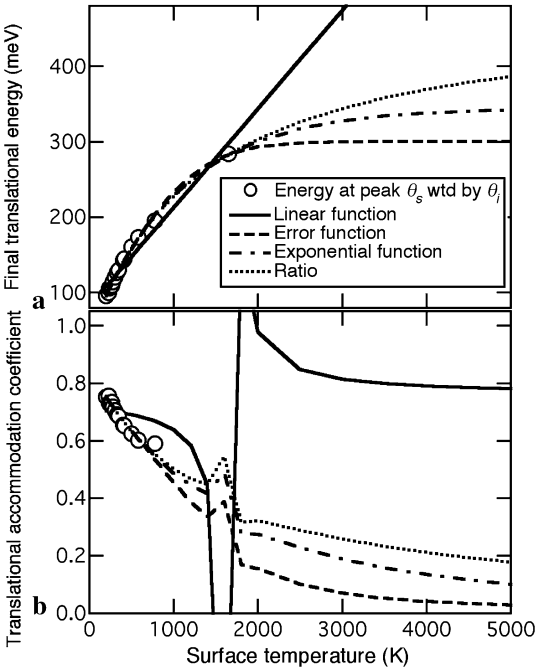

Fig. 8 Surface-temperature dependence of the (**a**) final translational energy and (**b**) translational accommodation coefficient for NO scattered from a graphite surface extrapolated to high surface temperatures. The circles in (**a**) are the same as those in Fig. 4b, and the circles in (**b**) are the same as those in Fig. 4c and are derived from measurements of Vach et al. [15]. The *lines* represent results of fits to the data in (**a**) using (17) (*solid line*), (18) (*dashed line*), (19) (*dot-dashed line*), and (20) (*dotted line*). The fit parameters are given in Table 4, and the fits in (**a**) were used to derived the lines in (**b**)

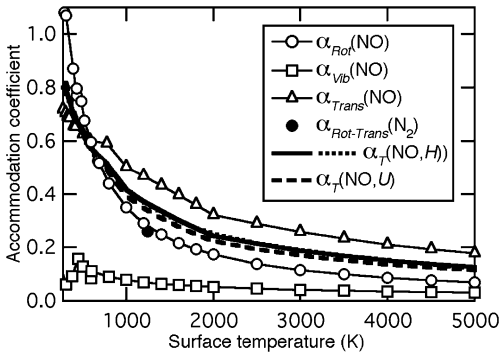

Fig. 9 Surface-temperature dependence of the partial accommodation coefficients for translational, rotational, and vibrational degrees of freedom of NO scattered from a graphite surface. *Open symbols* represent values derived from measurements from Häger, Walther, and coworkers [14–21] and extrapolated to higher surface temperatures, as described in the text. The *solid circle* is from Leroy et al. [13] for N_2 in which translation and rotation were probably equilibrated with each other via gas-phase collisions; the gas temperature was 293 K. The *solid line* was derived using (11), and the *dashed line* was derived using (12). The *dotted line* (barely visible) is a fit to the *solid line*. Values of the points shown are given in Tables 1–3

tion of surface temperature are not complete enough to derive translational accommodation coefficients.

3.1.4 Combined dependence of α_T on surface temperature

In general thermal accommodation appears to decrease with increasing surface temperature at surface temperatures above that at which trapping/desorption is significant. The overall thermal accommodation coefficient of H_2 on graphite has been observed to increase with increasing surface temperature at low surface temperatures (77–340 K) [43] but decrease with increasing temperature at higher temperatures (from 0.82 at 77 K to 0.15 at 1,450 K) [13, 31, 43, 44], and those of Kr, Xe, and CH_4 have also been observed to decrease with increasing surface temperature from 850–1,400 K [31].

Figure 9 shows a comparison of values of rotational, vibrational, and translational accommodation coefficients for NO scattered from graphite extrapolated to high surface temperatures, as described above. The coupling between translational and rotational degrees of freedom is generally strong [22, 35], and translational and rotational accommodation coefficients are often assumed to be comparable. Figure 9 suggests that rotational accommodation is higher at low surface temperatures and lower at high surface temperatures than translational accommodation. Studies of NO/graphite scattering have shown very similar angular, rotational, and translational distributions for molecules scattering to and from different vibrational states, which indicates that rotational and translational degrees of freedom are decoupled from vibrational degrees of freedom for this system [15]. The results of this study suggested that all degrees of freedom were strongly coupled to surface phonons. In general vibrational accommodation tends to be significantly lower than accommodation of translational and rotational degrees of freedom, particularly for molecules with large vibrational spacings, which is consistent with the re-

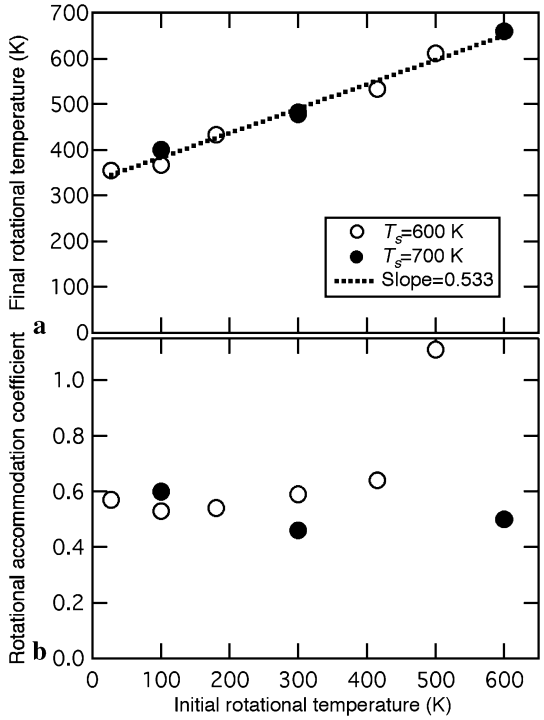

Fig. 10 Dependence of the (**a**) final rotational temperature and (**b**) rotational accommodation coefficient on initial rotational temperature of NO scattered from a graphite surface. The *symbols* in (**a**) represent data from Häger et al. [14], from which the *points* in (**b**) were derived. The data were recorded with an incidence energy of 124 meV and incidence angle of 45° at surface temperatures of 600 and 700 K as indicated in the legend. The *dotted line* in (**a**) shows a linear fit to the data

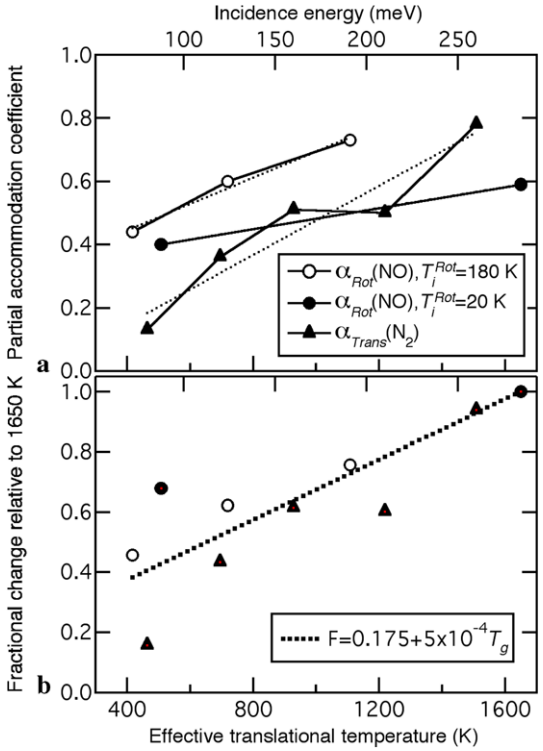

Fig. 11 Effective gas-temperature dependence of the accommodation coefficients for translational and rotational degrees of freedom of NO and N_2 scattered from a graphite surface. *Circles* represent values derived from measurements of NO at a surface temperature of 600 K from Häger et al. [14] for an incidence angle of 45° and initial rotational temperature of 180 K (*open circles*) and from Häger et al. [20, 21] for an incidence angle of 70° and initial rotational temperature of 20 K (*solid circles*). *Solid triangles* represent values derived from measurements of N_2 at a surface temperature of 293 K and incidence angle of 60° from Kinefuchi et al. [25]. (**a**) Partial accommodation coefficients are shown as a function of effective translational temperature, which is assumed to be associated with the gas temperature according to $T_g \approx T_i^{\text{Trans}} \equiv E_i/2k_B$. These values are given in Tables 5 (*circles*) and 7 (*triangles*). The *dotted lines* show linear fits to each data set. (**b**) Values from (**a**) were scaled to unity at 1,650 K using the predicted values at 1,650 K from the linear fits. The *dotted line* shows a fit to the combined scaled data set to derive a gas-temperature scaling factor

sults shown in Fig. 9. Surface roughness will also have an effect. The surface roughness of diamond(111) or sputtered carbon is much higher than for graphite, trapping is more effective, and accommodation coefficients are larger [29, 45].

Equation (11) or (12) can be used to derive an overall accommodation coefficient as a function of surface temperature from these data. The results of these calculations are also shown in Fig. 9. An exponential decay with a sloping baseline (dotted line) does a good job of fitting the curve derived from (11) (solid line) and yields

$$\alpha_T(H, T_S) = \left[0.28 - 3.23 \times 10^{-5} T_S + 0.800 \exp\left(-1.53 \times 10^{-3} T_S\right)\right]. \quad (23)$$

The data used to derive this equation were recorded at an effective gas temperature ($T_g = E_i/2k_B$) of 1,650 K.

3.2 Dependence of α_T on gas temperature

3.2.1 Dependence of α_{Rot} on gas temperature

Because T_f^{Rot} depends on neither initial vibrational state [20, 21] nor incidence angle [17, 18], only the incidence energy and initial rotational temperature need to be considered in determining the effect of gas temperature on the final rotational temperature and rotational accommodation coefficient. Figure 1 shows that, at high surface temperatures, T_f^{Rot} and α_{Rot} depend on incidence energy, which is associated with a translational temperature of the incoming gas molecules. The final rotational temperature also depends on the initial rotational temperature. Figure 10a shows that, for a fixed incidence energy, T_f^{Rot} increases linearly with T_i^{Rot}. A linear fit to the data yields a slope of 0.533. Figure 10b shows the corresponding rotational accommodation coefficient as a function of initial rotational temperature. Although T_f^{Rot} increases linearly with T_i^{Rot}, α_{Rot} is nearly independent of T_i^{Rot} at higher surface temperatures, as long as the rotational temperature is significantly different from the surface temperature. These plots were derived from data given in

Figs. 5 and 6 of Häger et al. [14] for an incidence energy of 124 meV, incidence angle of 45°, and surface temperatures of 600 and 700 K.

There are fewer data points to use to assess the impact of translational temperature on α_{Rot}. Figure 11a shows α_{Rot} plotted as a function of the effective translational temperature, which is assumed to correspond to the gas temperature and is approximated from the incidence energy using the expression $T_g \approx T_i^{\mathrm{Trans}} \approx E_i/2k_B$. Values of α_{Rot} were derived from data taken from Fig. 4 of Häger et al. [14] and Fig. 8 of Häger and Walther [21] for a surface temperature of 600 K. Values are given in Table 5. The data indicate an increase in α_{Rot} with increasing T_i^{Trans}.

3.2.2 *Dependence of* α_{Vib} *on gas temperature*

The results in Fig. 2c demonstrate little dependence of α_{Vib} on the initial vibrational temperature. In addition, there appears to be very little coupling between molecular vibrational and other molecular degrees of freedom for the NO/graphite system. The vibrational state of the incident or scattered molecules does not appear to influence the rotational temperature, velocity distribution, or angular distribution of the scattered molecules [15, 20, 21]. The results of Vach et al. [15, 20] suggest that vibrational accommodation proceeds via close coupling between the molecular vibrational degree of freedom and those of surface phonons. These results indicate that the vibrational accommodation coefficient does not depend on gas temperature.

Figure 3 shows α_{Vib} for CF_3Br scattered from a graphite surface at two significantly different incidence energies. Even for the CF_3Br/graphite system, for which exchange of vibrational energy with the surface is relatively efficient, there appears to be little dependence on incidence energy. At much higher incidence energies there appears to be an increase in the vibrational accommodation coefficient with incidence energy for both CF_3Br [36, 37] and SF_6 [38] (see Table 6), but these energies correspond to effective translational temperatures exceeding 14,000 K, which is beyond the range of interest for the present study.

3.2.3 *Dependence of* α_{Trans} *on gas temperature*

The available data are limited for assessing the effect of gas temperature on α_{Trans}. As shown above, relatively comprehensive data sets have been published for the NO/graphite system at incidence velocities of 750 and 1,350 m/s, but most of the data at 750 m/s were recorded at a surface

Table 5 Rotational accommodation coefficients inferred from gas-surface scattering measurements on graphite over a range of effective gas temperatures

Species	T_S (K)	T_i^{Rot} (K)	T_f^{Rot} (K)	E_i (meV)	T_g (K)	α_{Rot}	Reference
NO	600	180	365	72	417	0.44	Fig. 4 of [14]
	600	180	430	124	719	0.60	
	600	180	485	191	1,110	0.73	
NO	600	20	255	87.5	508	0.40	Fig. 2 of [20]
	600	20	362	284	1,650	0.59	Fig. 8 of [21]

Table 6 Vibrational accommodation coefficients inferred from gas-surface scattering measurements on graphite over a range of effective gas temperatures

Species	T_S (K)	T_i^{Vib} (K)	T_f^{Vib} (K)	E_i (meV)	T_g (K)	α_{Vib}	Reference
CF_3Br	830	320	427	690	4,000	0.21	Table 1 of [36]
	830	320	460	1,560	9,050	0.27	
	830	320	484	2,450	14,200	0.32	
CF_3Br	830	300	438	500	2,900	0.26	Fig. 5 of [37]
	830	300	430	1,500	8,700	0.24	
	830	300	430	1,900	11,000	0.24	
	830	300	450	2,500	14,500	0.28	
	830	300	510	4,000	23,200	0.40	
	830	300	550	5,250	30,500	0.47	
SF_6	1,170	300	318	640	3,710	0.021	Fig. 2 of [38]
	1,170	300	324	1,420	8,120	0.028	
	1,170	300	354	2,500	14,500	0.062	

Table 7 Translational accommodation coefficients inferred from gas-surface scattering measurements on graphite over a range of effective gas temperatures

Species	T_S (K)	E_S (meV)	E_f (meV)	E_i (meV)	T_g (K)	α_{Trans}	Reference
N_2	293	50	76	80	460	0.13	Fig. 5 of [25]
	293	50	95	120	700	0.36	$\theta_i = 60°$
	293	50	104	160	930	0.51	
	293	50	130	210	1,220	0.50	
	293	50	96	260	1,510	0.78	
Xe	550	95	238	450	2,610	0.60	Figs. 2 & 3 of [42]
	550	95	766	1,560	9,050	0.54	Figs. 3 & 4 of [46]
	550	95	1,709	3,620	21,000	0.54	$\theta_i = 35°$

temperature of 500 K, for which $E_s \approx E_i$ and values of α_{Trans} are unreliable. There are some data available for N_2 scattered from graphite, as shown in Fig. 11a and tabulated in Table 7. This data set is not as complete as that for NO/graphite, and correction for the effect of incidence angle is not possible. Nevertheless, the data set provides some information about the effect of incidence energy on accommodation at a single incidence angle of 60° and a surface temperature of 293 K. The results suggest that α_{Trans} increases with increasing gas temperature for N_2 scattered from graphite.

As noted above, measurements of Xe scattered from graphite surfaces are also not complete enough to derive an accommodation coefficient. At a single incidence angle of 35°, however, the translational accommodation of Xe [42, 46] on graphite appears to be approximately independent of incidence translational energy (see Table 7). These data were taken at relatively high incidence energies for which the effective translational temperatures were between 2,600 and 21,000 K.

3.2.4 Combined dependence of α_T on gas temperature

In general, thermal accommodation tends to increase with increasing incidence translational energy, i.e., gas temperature. The available data sets are not complete enough even for NO/graphite, however, to generate an overall accommodation coefficient as a function of effective gas temperature, such as that generated as a function of surface temperature and shown in Fig. 9. In order to estimate the dependence on gas temperature, each data set in Fig. 11a was fit to a line (dotted lines) and scaled to unity at an effective translational temperature of 1,650 K, as shown in Fig. 11b. The fractional change was inferred by a global linear fit to the scaled data (dotted line in Fig. 11b). The result is a multiplicative factor that lowers the accommodation coefficient at gas temperatures below 1,650 K and increases it above this gas temperature.

3.3 Grand finale

Including the gas-temperature correction factor in (23) yields

$$\alpha_T(H, T_S, T_g) = \left[0.28 - 3.23 \times 10^{-5} T_S + 0.800 \exp\left(-1.53 \times 10^{-3} T_S\right)\right] \times (0.175 + 5 \times 10^{-4} T_g). \quad (24)$$

The corresponding expression for U is

$$\alpha_T(U, T_S, T_g) = \left[0.28 - 3.50 \times 10^{-5} T_S + 0.934 \exp\left(-1.82 \times 10^{-3} T_S\right)\right] \times \left(0.175 + 5 \times 10^{-4} T_g\right). \quad (25)$$

The difference between (24) and (25) is small, as shown in Fig. 9.

Equations (24) and (25) predict a value for α_T of 0.18–0.19 for a gas temperature of 1,900 K and surface temperature of 3,500 K. This value is lower than the range of values (0.23–0.37) often used in LII models, for which these gas and surface temperatures are typical [4].

Validation of this accommodation coefficient would involve comparison with total accommodation coefficient measurements of NO on graphite at defined surface and gas temperatures, which are currently unavailable. Confirmation would also benefit from measurements of other gases with graphite, particularly diatomics and especially N_2. Overall accommodation coefficients are available for H_2 and O_2 [31, 43, 44], but both of these species tend to dissociate on graphite at higher temperatures.

4 Conclusions

State-to-state scattering measurements were used to derive an expression for the overall accommodation coefficient of NO with graphite as a function of surface temperature and

gas temperature. The resulting expression, when extrapolated to surface and gas temperatures frequently encountered during LII measurements, yields an estimate for the accommodation coefficient of 0.18–0.19, which is lower than the range of values often used in LII models [4]. Useful measurements for validating and extending this analysis would include (1) state-to-state measurements of NO scattered from graphite at higher surface temperatures and as a function of incidence energy, (2) state-to-state measurements of other gases, particularly N_2, scattered from graphite, (3) overall accommodation coefficients of relevant species with graphite under well-defined conditions, and (4) measurements on both single crystal and polycrystalline graphite surfaces.

Acknowledgements I thank Tom Settersten for enlightening discussions about energy transfer. This work was funded by the Division of Chemical Sciences, Geosciences, and Biosciences, the Office of Basic Energy Sciences, the US Department of Energy. Sandia is a multiprogram laboratory operated by Sandia Corporation, a Lockheed Martin Company, for the National Nuclear Security Administration under contract DE-AC04-94-AL85000.

References

1. L.A. Melton, Appl. Opt. **23**, 2201 (1984)
2. R.J. Santoro, C.R. Shaddix, Laser-induced incandescence, in *Applied Combustion Diagnostics*, ed. by K. Kohse-Höinghaus, J.B. Jeffries (Taylor & Francis, New York, 2002), pp. 252–286
3. C. Schulz, B.F. Kock, M. Hofmann, H.A. Michelsen, S. Will, B. Bougie, R. Suntz, G.J. Smallwood, Appl. Phys. B **83**, 333 (2006)
4. H.A. Michelsen, F. Liu, B.F. Kock, H. Bladh, A. Boiarciuc, M. Charwath, T. Dreier, R. Hadef, M. Hofmann, J. Reimann, S. Will, P.-E. Bengtsson, H. Bockhorn, F. Foucher, K.P. Geigle, C. Mounaïm-Rousselle, C. Schulz, R. Stirn, B. Tribalet, R. Suntz, Appl. Phys. B **87**, 503 (2007)
5. F.O. Goodman, Prog. Surf. Sci. **5**, 261 (1974)
6. F.O. Goodman, H.Y. Wachman, *Dynamics of Gas-Surface Scattering* (Academic, New York, 1976)
7. T. Lehre, B. Jungfleisch, R. Suntz, H. Bockhorn, Appl. Opt. **42**, 2021 (2003)
8. K.J. Daun, G.J. Smallwood, F. Liu, J. Heat Transfer **130**, 121201 (2008)
9. S.-A. Kuhlmann, J. Reimann, S. Will, J. Aerosol Sci. **37**, 1696 (2006)
10. F. Liu, M. Yang, F.A. Hill, D.R. Snelling, G.J. Smallwood, Appl. Phys. B **83**, 383 (2006)
11. D.R. Snelling, F. Liu, G.J. Smallwood, Ö.L. Gülder, Combust. Flame **136**, 180 (2004)
12. R. Starke, B. Kock, P. Roth, Shock Waves **12**, 351 (2003)
13. O. Leroy, J. Perrin, J. Jolly, M. Péalat, M. Lefebvre, J. Phys. D: Appl. Phys. **30**, 499 (1997)
14. J. Häger, D. Glatzer, H. Kuze, M. Fink, H. Walther, Surf. Sci. **374**, 181 (1997)
15. H. Vach, J. Häger, H. Walther, J. Chem. Phys. **90**, 6701 (1989)
16. J. Häger, Y.R. Shen, H. Walther, Phys. Rev. A **31**, 1962 (1985)
17. J. Häger, H. Walther, J. Vac. Sci. Technol. B **3**, 1490 (1985)
18. J. Häger, H. Walther, Nucl. Instrum. Methods Phys. Res. Sect. A **239**, 425 (1985)
19. H. Kuze, J. Häger, H. Walther, Chem. Phys. Lett. **153**, 569 (1988)
20. H. Vach, J. Häger, H. Walther, Chem. Phys. Lett. **133**, 279 (1987)
21. J. Häger, H. Walther, Annu. Rev. Mater. Sci. **19**, 265 (1989)
22. C.T. Rettner, D.J. Auerbach, J.C. Tully, A.W. Kleyn, J. Phys. Chem. **100**, 13021 (1996)
23. F. Pradére, A. De Martino, C. Flytzanis, Proc. Indian Acad. Sci. (Chem. Sci.) **103**, 237 (1991)
24. S.I. Ionov, M.E. LaVilla, R.S. Mackay, R.B. Bernstein, J. Chem. Phys. **93**, 7406 (1990)
25. I. Kinefuchi, H. Yamagachi, S. Shiozaki, Y. Sakiyama, Y. Matsumoto, Out-of-plane scattering distribution of nitrogen molecular beam on graphite (0001) surface, in *Rarefied Gas Dynamics: 24th International Symposium* (American Institute of Physics, 2005)
26. F. Frenkel, J. Häger, W. Krieger, H. Walther, G. Ertl, J. Segner, W. Vielhaber, Chem. Phys. Lett. **90**, 225 (1982)
27. J. Häger, M. Fink, H. Walther, Surf. Sci. **550**, 35 (2004)
28. J. Segner, H. Robota, W. Vielhaber, G. Ertl, F. Frenkel, J. Häger, W. Krieger, H. Walther, Surf. Sci. **131**, 273 (1983)
29. C.T. Rettner, IEEE Trans. Magn. **34**, 2387 (1998)
30. P.L. Houston, R.P. Merrill, Chem. Rev. **88**, 657 (1988)
31. S.C. Saxena, R.K. Joshi, *Thermal Accommodation and Absorption Coefficients of Gases* (McGraw–Hill, New York, 1981)
32. H.A. Michelsen, M.A. Linne, B.F. Kock, M. Hofmann, B. Tribalet, C. Schulz, Appl. Phys. B **93**, 645 (2008)
33. R.S. Berry, S.A. Rice, J. Ross, *Physical Chemistry* (Wiley, New York, 1980)
34. J.B.C. Pettersson, G. Nyman, L. Holmlid, J. Chem. Phys. **89**, 6963 (1988)
35. G. Nyman, L. Holmlid, J.B.C. Pettersson, J. Chem. Phys. **93**, 845 (1990)
36. M.B. Andersson, J.B.C. Pettersson, N. Marković, Surf. Sci. **384**, L880 (1997)
37. M.B. Någård, N. Marković, J.B.C. Pettersson, J. Chem. Phys. **109**, 10350 (1998)
38. M.B. Andersson, J.B.C. Pettersson, Chem. Phys. Lett. **250**, 555 (1996)
39. M. van Opbergen, A. Boschetti, S. Iannotta, Opt. Express **4**, 53 (1999)
40. K.C. Janda, J.E. Hurst, C.A. Becker, J.P. Cowin, D.J. Auerbach, L. Wharton, J. Chem. Phys. **72**, 2403 (1980)
41. K.C. Janda, J.E. Hurst, J.P. Cowin, L. Wharton, D.J. Auerbach, Surf. Sci. **130**, 395 (1983)
42. H.Y. Watanabe, H. Yamaguchi, M. Hashinokuchi, K. Sawabe, S. Maruyama, Y. Matsumoto, K. Shobatake, Chem. Phys. Lett. **413**, 331 (2005)
43. I. Yasumoto, J. Phys. Chem. **91**, 4298 (1987)
44. K.L. Day, Int. Astron. Union Symp. **52**, 311 (1973)
45. Y. Matsuo, H. Vach, M. Châtelet, J. Häger, C. Roth, C. Flytzanis, H. Walther, J. Chem. Phys. **93**, 4368 (1990)
46. Y. Watanabe, H. Yamaguchi, M. Hashinokuchi, K. Sawabe, S. Maruyama, Y. Matsumoto, K. Shobatake, Eur. Phys. J. D **38**, 103 (2006)